sity by a factor of 2 in this-time interval.

In conclusion, we have demonstrated the recording of transient x-ray line intensities and line shapes from laser-produced plasmas. Observations of this type have considerable potential for (a) verifying or correcting conclusions based on line shapes and intensity ratios in time-integrated spectra and (b) providing time scales for such topically interesting processes as implosion of microballoons, burn through by ablation of layers of material where the layers are identifiable by spectrally adjacent characteristic x-ray lines,[8] and mixing through hydrodynamic instabilities in similarly identifiable layers in ablatively imploded laser fusion targets.

It is a pleasure to acknowledge the contribution of E. Bateman in developing the more sensitive low-density CsI x-ray photocathode. This work was supported by the Science Research Council.

[a]Present address: Science Research Council Rutherford and Appleton Laboratory, Chilton, Didcot, Oxon, OX11 0QX, United Kingdom.

[1]V. A. Boiko, S. A. Pikuz, and A. Ya Faenov, J. Phys. B 12, 1889 (1979).

[2]J. M. Auerbach *et al.*, J. Appl. Phys. 50, 5478 (1979).

[3]B. Yaakobi *et al.*, Phys. Rev. A 19, 1247 (1979).

[4]M. H. Key, J. G. Lunney, J. M. Ward, R. G. Evans, and P. T. Rumsby, J. Phys. B 12, L213 (1978).

[5]K. B. Mitchell, D. B. Van Huysteyn, G. M. McCall, P. Lee, and H. R. Griem, Phys. Rev. Lett. 42, 232 (1979).

[6]M. H. Key, M. J. Lamb, C. L. S. Lewis, A. Moore, and R. G. Evans, Appl. Phys. Lett. 34, 550 (1979).

[7]P. H. Lee and M. D. Rosen, Phys. Rev. Lett. 42, 236 (1979); P. T. Attwood *et al.*, Phys. Rev. Lett. 37, 499 (1976).

[8]Annual report to the Laser Facility Committee, Science Research Council Rutherford and Appleton Laboratory Report No. RL 79-036, 1979 (unpublished).

[9]V. A. Boiko, A. Yu. Chugunov, A. Ya. Faenov, S. A. Pikuz, I. Yu. Skobelev, A. Vinogradov, and E. A. Yukov, J. Phys. B 12, 213 (1979).

[10]C. P. Bhalla, A. H. Gabriel, and L. P. Presnyakov, Mon. Not. Roy. Astron. Soc. 172, 359 (1975).

[11]J. L. Weisheit, C. B. Tarter, J. M. Schofield, and L. M. Richards, J. Quant. Spectros. Radiat. Transfer 16, 559 (1976).

Compression of Polymer-Coated Laser-Fusion Targets to Ten Times Liquid DT Density

J. M. Auerbach, W. C. Mead, E. M. Campbell, D. L. Matthews, D. S. Bailey, C. W. Hatcher, L. N. Koppel, S. M. Lane, P. H. Y. Lee, K. R. Manes, G. McClellan, D. W. Phillion, R. H. Price, V. C. Rupert, V. W. Slivinsky, and C. D. Swift

Lawrence Livermore Laboratory, University of California, Livermore, California 94550

(Received 10 March 1980)

Polymer-coated glass microspheres filled with DT fuel and argon seed gas were irradiated with the SHIVA 1.06-μm laser using 4-kJ, 200-ps (full width at half maximum), Gaussian pulses. Measured light absorption, x-ray spectrum, neutron yields, and x-ray continuum images compared favorably with detailed computer simulations. Pusher neutron activation and argon line imaging diagnostics were utilized to measure fuel density. Fuel densities of 1–3 g/cm^3 or 5–15 times liquid DT density were inferred.

PACS numbers: 52.50.Jm, 52.55.Pi

Recently, much laser-driven inertial-confinement-fusion (ICF) research has turned towards the next step in achieving high-gain targets: compressing DT to high density.[1] Earlier efforts concentrated on short-pulse (< 100 ps) exploding-pusher targets[2] which achieved high final DT temperatures (2–8 keV) but low DT densities (~ 0.2 g/cm^3). However, to achieve high gain for an ICF reactor, low-isentrope, ablatively driven implosions are required to compress DT to high densities (> 200 g/cm^3).

The work reported here employed thick-walled, coated microspheres, intermediate pulse lengths, and fairly high laser irradiance to operate between these two regimes. The target designed for these experiments is shown in Fig. 1. The twenty SHIVA beams were tangentially focused with p polarization. With 4 kJ incident in a 200-ps Gaussian pulse, intensities at the poles (near the beam-cluster axis) and the equator were ~ 4 $\times 10^{15}$ W/cm^2, while at intermediate latitudes, intensities were ~ 2$\times 10^{16}$ W/cm^2.

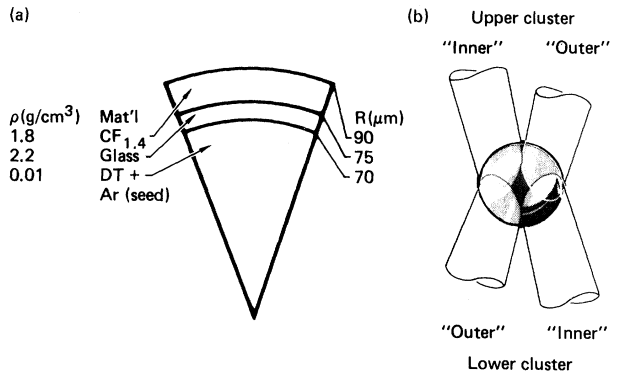

FIG. 1. (a) Target design and (b) illumination diagrams.

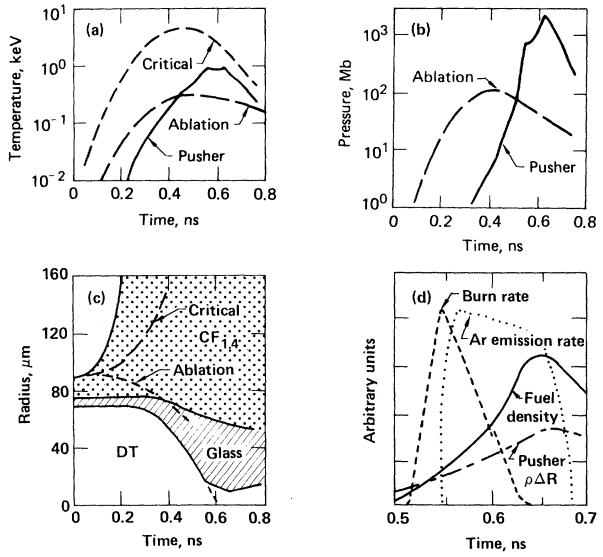

FIG. 2. LASNEX-calculated histories: (a) temperatures; (b) pressures; (c) radii; and (d) detailed stagnation timing.

Simulations of the performance of this target have been performed using the hydrodynamic code LASNEX[3] in one and two dimensions. Recent improvements include a more detailed scaling for suprathermal electrons produced by resonance absorption[4] and a solution of the full nonlocal-thermodynamic-equilibrium ionization and radiation rate equations.[5]

The one-dimensional (1D) calculated time histories for pusher and ablator temperatures, pressures, and radii are presented in Fig. 2. We calculate that ~50% of the incident light is backscattered before reaching the critical surface and 20% absorption occurs mainly by resonant absorption. Suprathermally heated electrons are produced at an effective temperature of 30 keV. The implosion compresses the DT to a final density of 2–3 g/cm^3 and a peak temperature of > 3 keV for ions and ~ 1 keV for electrons. Calculated neutron yields are 10^8–10^9, showing moderately strong sensitivity to model assumptions.

Since this design operates at fairly high shock and preheat levels, the implosion stagnation is mistimed. As seen in Fig. 2(c), the incoming pusher is first sharply decelerated as a large stagnation pressure develops in the DT fuel, then more gently slowed over the remainder of the compression. Thus, peak fuel ion and electron temperatures occur significantly before peak fuel compression, and, further, pusher-fuel mixing may occur at the unstable glass-DT interface. These complications introduce factor-of-2 model dependences into the inference of final density, as discussed below.

The data on absorption and heating support current theoretical models. Arrays of plasma calorimeters, laser calorimeters, and photodiodes provide two independent absorption measurements which indicate an absorption fraction of 0.23 ± 0.05. A filter fluorescer was used to measure the fluence of 50–80-keV x rays produced by bremsstrahlung of the suprathermal electrons. We measure a fluence of ~ 10^{-3} J/keV at $h\nu = 50$ keV and a slope of 24 keV (with uncertainty of a factor of 2), consistent with calculated values.

Neutron yields were measured with lead- and copper-activation detectors. For seven shots with average incident energy of 3.8 ± 0.4 kJ the average yield obtained was $3.1 \pm 0.5 \times 10^8$.

Determination of the compressed fuel density was the most formidable task in these experiments. Unfortunately, we cannot completely diagnose the fuel conditions. Instead, we use two complementary measurements,[6] supplemented by detailed modeling: (1) imaging of the x-ray line emission of Ar seed gas in the DT fuel and (2) neutron activation analysis of the glass pusher. We discuss each of these in turn.

Imaging the line emission from a seed gas mixed with the DT fuel provides a direct indication of fuel compression which is not available with x-ray continuum imaging. However, the line imaging used here was 1D; so we must supplement the measurement by continuum two-dimensional (2D) images and detailed simulations.

We have utilized a post-processor coupled to LASNEX to solve the ionization and radiation rate equations for an Ar seed gas at 0.3 atm partial

pressure. The core stagnation conditions efficiently populate the He-like Ar^{+16} ionization state. For the $1s2p(^1P_1) \rightarrow 1s^2(^1S_0)$ line at 3.14 keV, we calculate optically thin emission of $\sim 10^{17}$ keV/keV with attenuation 1/20 in transport through the compressed glass pusher. This gives net intensity a factor of ~3 above the calculated continuum background from the laser-heated corona and the compressed core. The Ar-line radiated power vs time is shown in Fig. 2(d).

An x-ray crystal spectrometer with high sensitivity and low energy dispersion was developed to image the Ar line emission. The crystal provided spectral resolution of about 10 eV in one film dimension, while a slit 20 μm wide yielded 25 μm spatial resolution in the other film dimension along the target pole-to-pole axis.

We obtained images of the Ar line on four shots, two of which were simultaneously diagnosed by radiochemistry. The actual Ar seed gas partial pressure was 0.05–0.10 atm, lower than optimal. The observed signal-to-noise ratio of 1.5–2.0 and the 25-μm spatial resolution introduce significant uncertainty into determining the spatial extent of the line emission. A plot of the line emission versus position is shown in Fig. 3(a) after continuum subtraction. The average linewidth [full width at half maximum (FWHM)] after slit deconvolution is 30 ± 5 μm.

We can determine characteristics of the heating and implosion symmetry using 2D continuum x-ray images. Here, we employ an equatorial-viewing x-ray microscope in the energy band 3.0–4.5 keV. A typical experimental image is shown in Fig. 3(b). We note clear evidence of enhanced polar heating, and an oblate stagnation image with widths (FWHM) of 28 μm vertically and 48 μm horizontally.

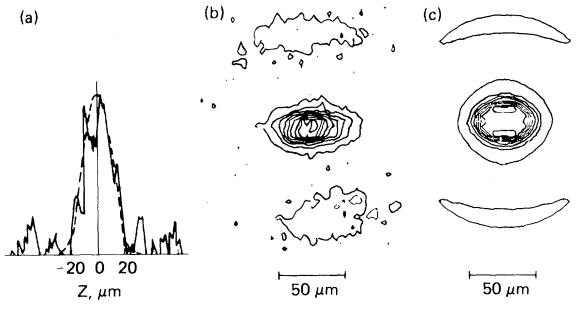

FIG. 3. X-ray images: (a) measured (solid line) and calculated (dashed line) 1D Ar line emission trace; (b) measured and (c) calculated 2D continuum x rays at ~3.5 keV.

A rough lower limit on the fuel density can be obtained from the Ar line image by assuming instantaneous, uniform emission from an ellipsoid of eccentricity 1.7:1, as estimated from the x-ray continuum image. This gives roughly 0.4–1.2 g/cm^3.

To infer a DT density more accurately, we compare detailed 2D LASNEX simulations to both the continuum image at ~3.5 keV and the Ar line emission image. These calculations, with the instrumental resolution folded in, are shown in Fig. 3(c) and 3(a), respectively. The 2D calculation attains a DT density of 2 g/cm^3 at peak compression, and matches (to ~15%) both the symmetry and extent of the continuum image and the extent of the Ar emission from the core. From this, we infer an average DT density of 0.8–3.5 g/cm^3 at peak compression.

Neutron activation analysis of the glass pusher is the most reliable density diagnostic available for current experimental conditions. From the measured cross section for the reaction ^{28}Si(n, p)^{28}Al, the measured number of activated ^{28}Al atoms A, and the neutron yield Y, we can calculate the effective pusher areal density (in g/cm^2) as $(\rho\Delta r)_{\rm eff} = 480A/Y$, where we have averaged over the burn time. We have performed this measurement on three target shots and obtain the mean value $(\rho\Delta r)_{\rm eff} = 5.8 \pm 1.0$ mg/cm^2.

A simple ideal-gas model can be used to relate the pusher $\rho\Delta r$ to the fuel density at burn time.

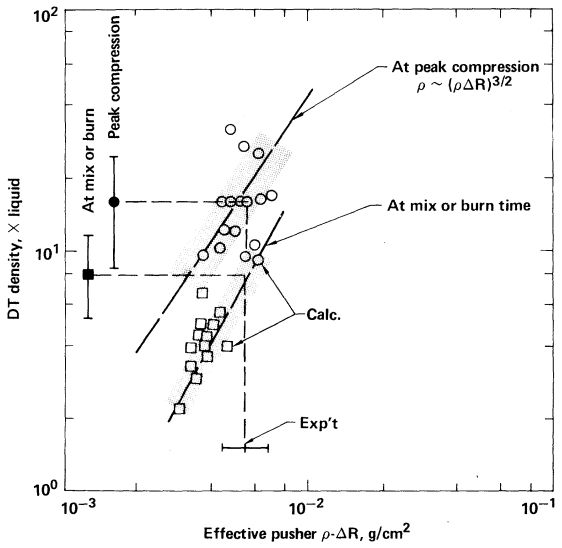

FIG. 4. Calculated fuel density vs pusher areal density $(\rho\Delta r)_{\rm eff}$, showing model dependence; experimental $(\rho\Delta r)_{\rm eff}$ and inferred fuel densities are shown.

TABLE I. Summary of density determination results.

Argon line imaging results	
Image width (FWHM), μm	30 ± 5
Eccentricity (continuum)	1.7 ± 0.2
Inferred DT density, g/cm^3	
at peak compression	$2.0^{+1.5}_{-1.2}$
Radiochemical activation results	
Pusher areal density, mg/cm^2	5.8 ± 1.0
Inferred DT density, g/cm^3	
at peak burn	$1.6^{+0.9}_{-0.6}$
at peak compression	$3.3^{+2.6}_{-1.5}$

Assuming that a fraction ϵ of the initial pusher mass surrounds the fuel in a spherical, isothermal, isobaric core, we obtain $\rho_f \approx 2000\epsilon^{-0.9} \times (\rho\Delta r)_p^{1.5}$ (cgs units), for the pellet configuration used here. We can also use this simple model to estimate the fuel density attained experimentally. Taking $\epsilon = 0.5$, we obtain fuel densities of 1.5–2.5 g/cm^3 from the measured $\rho\Delta r$. With $\epsilon = 1$, we obtain a rough lower limit to the densities of 0.8–1.4 g/cm^3.

The LASNEX simulations allow more detailed modeling of the activation dynamics, as shown in Fig. 2(d). The plot of Fig. 4 gives the relationship between DT density and pusher areal density at two times; peak burn rate and peak DT compression. The densities differ by about a factor of 2, with the latter density significantly more model-dependent than the former. Two-dimensional effects may modify the density attained, but affect the ρ vs $(\rho\Delta r)_{\text{eff}}$ relationship only in quite pathological cases. From Fig. 4, we infer densities of 1.0–2.5 g/cm^3 at peak burn, and 1.8–5.9 g/cm^3 at peak compression.

The results presented have demonstrated the feasibility of a number of design and experimental ideas. We have used polymer-coated targets to produce a moderate-isentrope, partly ablatively driven implosion. We have found good agreement with detailed simulations based on familiar plasma processes. We have simultaneously used multiple diagnostics to determine the density of the imploded fuel. The results, summarized in Table I, strongly support compression of DT to more than 2 g/cm^3 or ten times liquid DT density.

The need for more complete diagnosis of the imploded configuration can be seen. Other experiments at higher densities are in progress.

The authors thank H. Ahlstrom and J. H. Nuckolls for their guidance and support. The target fabrication group and the SHIVA operations crew have contributed immeasurably. This work was supported by the U. S. Department of Energy under Contract No. W-7405-ENG-48.

[1]N. G. Basov *et al.*, in *Plasma Physics, Nonlinear Theory and Experiment*, edited by H. Wilhelmsson (Plenum, New York, 1977), p. 47; T. Henderson and R. R. Johnson, Appl. Phys. Lett. 31, 18 (1977); R. A. Kopp, Bull. Am. Phys. Soc. 23, 808 (1978); W. C. Mead *et al.*, Lawrence Livermore Laboratory Report No. UCRL-83163, 1979 (unpublished); B. Yaakobi *et al.*, Phys. Rev. Lett. 44, 1072 (1980).

[2]G. Charatis *et al.*, in *Proceedings of the Fifth International Conference on Plasma Physics and Controlled Nuclear Fusion Research, Tokyo, Japan, 1974* (International Atomic Energy Agency, Vienna, 1975), Vol. II, p. 317; H. G. Ahlstrom *et al.*, *ibid.*, p. 375; M. Lubin *et al.*, *ibid.*, p. 459; D. R. Speck *et al.*, Lawrence Livermore Laboratory Report No. UCRL-82117, 1979 (unpublished).

[3]G. B. Zimmerman, Lawrence Livermore Laboratory Report No. UCRL-75881, 1974 (unpublished); G. B. Zimmerman and W. L. Kruer, Comments Plasma Phys. Controlled Fusion 2, 85 (1975).

[4]E. J. Valeo and W. L. Kruer, Phys. Rev. Lett. 33, 750 (1974); J. M. Kindel, K. Lee, and E. L. Lindman, Phys. Rev. Lett. 34, 134 (1975).

[5]G. B. Zimmerman, in *Laser Program Annual Report –1977*, Lawrence Livermore Laboratory Report No. UCRL-50021-77, 1978, Vol. II, p. 4–31.

[6]L. N. Koppel *et al.*, Lawrence Livermore Laboratory Report No. UCRL-83313, 1979 (unpublished); E. M. Campbell *et al.*, Lawrence Livermore Laboratory Report No. UCRL-83096, 1979 (unpublished).

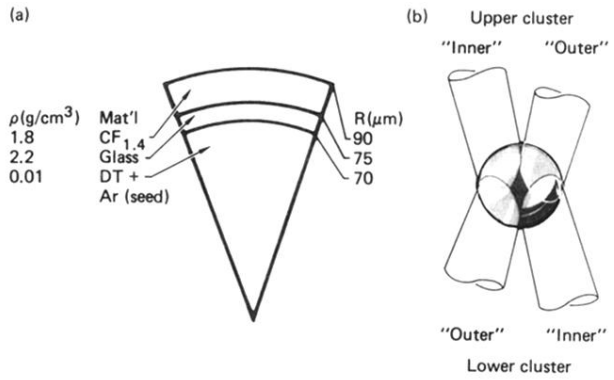

FIG. 1. (a) Target design and (b) illumination diagrams.